

Structure and mechanical properties of aluminum alloy/Ag interlayer/steel non-centered electron beam welded joints

ZHANG Bing-gang¹, CHEN Guo-qing¹, ZHANG Chun-guang¹, NI Jia-qiang²

1. State Key Laboratory of Advanced Welding and Joining, Harbin Institute of Technology, Harbin 150001, China;
2. AVIC Shenyang Aircraft Corporation, Shenyang 110034, China

Received 5 January 2011; accepted 11 May 2011

Abstract: Electron beam welding was carried out between aluminum alloy and steel with Ag interlayer. Seam morphology, structure and mechanical properties of the joints were investigated with different action positions of the electron beam spot. The results show that with the increment of the beam offset to the silver side from the interface between silver and steel, the seam morphology was improved, and the porosity in the Ag interlayer vanished. A transition layer mainly composed of Ag_2Al and Al eutectic was formed at the interface between silver and aluminum, and became thin and spicato as the beam offset increased. When the beam offset was too large, two IMC layers composed of $FeAl$ and $FeAl_3$ respectively were formed at the interface between steel and Ag interlayer. The optimal beam offset was 0.2 mm, and the maximum tensile strength of the joint was 193 MPa, 88.9% that of the aluminum alloy, and the fracture occurred at the interface between steel and Ag interlayer.

Key words: aluminum alloy; steel; Ag interlayer; non-centered electron beam welding; joint

1 Introduction

Aluminum alloys are being more and more used in light weight structures thanks to low density, high specific strength and good resistance against corrosion. Nowadays, aluminum alloy/steel components are widely used in fields of automotive, shipping, airspace and aerospace industries [1–2]. However, as a typical dissimilar metal assembly, there are problems of residual stress and brittle intermetallic phases in the joint because of their poor physical and metallurgical compatibility, which makes it difficult to join them together by traditional fusion welding technique. Other methods, such as diffusion bonding [3], friction stir welding [4–7], brazing [8–11], fusion-brazing [12–15], can produce joints with no defects. The joint by diffusion bonding has many advantages, such as good resistance to high temperature. The joint by friction stir welding possesses such advantages as homogeneous and compact microstructure, no gas pole and crack. The joint of brazing and fusion-brazing possesses such advantages as

little IMC, small distortion and high dimensional accuracy. But their application range is constrained because of their weak points such as joint format, producing efficiency or mechanical properties.

In this study, electron beam welding was carried out between aluminum alloy and steel with Ag as the interlayer, the microstructure of the joint with different action positions of the electron beam spot was analyzed, and the phase at the silver/steel interface was specially characterized. The mechanical properties were evaluated, and the optimal beam offset and maximum tensile strength were acquired.

2 Experimental

The body materials used in the experiments were 5A02 aluminum alloy and 0Cr18Ni9 stainless steel, and their chemical compositions are shown in Tables 1 and 2 respectively, and the main physical properties are listed in Table 3. The tensile strength of 5A02 is 217 MPa, with an elongation of 23%, and the tensile strength of 0Cr18Ni9 is 520 MPa, with an elongation of 40%.

Table 1 Chemical compositions of 5A02 aluminum alloy (mass fraction, %)

Si	Fe	Cu	Mn	Mg	Ti	Al
0.40	0.40	0.10	0.15–0.40	2.0–2.8	0.15	Bal.

Table 2 Chemical compositions of 0Cr18Ni9 steel (mass fraction, %)

C	Si	Mn	P	S	Ni	Cr	Fe
≤0.07	≤1.00	≤2.00	≤0.035	≤0.030	8.00–11.00	17.00–19.00	Bal.

Table 3 Physical properties of 5A02 and 0Cr18Ni9

Material	Density/ (g·cm ⁻³)	Melting point/ °C	Linear expansibility/ (10 ⁻⁶ K ⁻¹)	Specific heat capacity/(J·kg ⁻¹ ·K ⁻¹)	Heat conductivity/ (W·m ⁻¹ ·K ⁻¹)
5A02	2.68	652–627	25.4	1089	167.5
0Cr18Ni9	7.93	1 398–1 454	18.0	502	21.4

The body material specimens were rectangular, with 80 mm in length, 35 mm in width and 2 mm in thickness. The purity of the silver interlayer was more than 99.5%, and the size was 80 mm in length, 2 mm in width and 1 mm in thickness.

The body materials and the interlayer were burnished on the touching face and the neighboring zone using 200#, 600#, and 1000# SiC sand paper orderly before welding, and then were cleaned with acetone. The butt assembly of aluminum alloy/Ag interlayer/steel was mounted by a self-made clamp, and the gap between the touching faces was not more than 0.1 mm. The welding process was implemented in a vacuum electron beam welding machine. The welding parameters were as follows: accelerating voltage of 55 kV, focusing current of 2450 mA (upper surface focusing state), beam current of 11 mA, welding rate of 360 mm/min. Assuming d_s as the beam offset to the silver side from the interface between the silver and steel. In the experiments, d_s was 0, 0.2 mm, 0.3 mm, 0.4 mm respectively.

The structure of the weld and the morphology of the fractures were characterized on a scanning electron microscope (SEM). Chemical compositions of the correlative microstructure and the fractures were determined by energy dispersive X-ray spectrometer (EDX). The tensile strength of the welded joints was measured on an electronic universal testing machine. Three specimens of every seam were tested at the tensile speed of 1.0 mm/min. The average tensile strength was calculated from them to estimate the mechanical properties of the joints.

3 Results and discussion

3.1 Morphology of seam under different beam offsets

The morphologies of the seams under different beam offsets are shown in Fig. 1. When the beam spot acted at the interface between the silver interlayer and steel (Fig. 1(a)), both the steel and the interface were

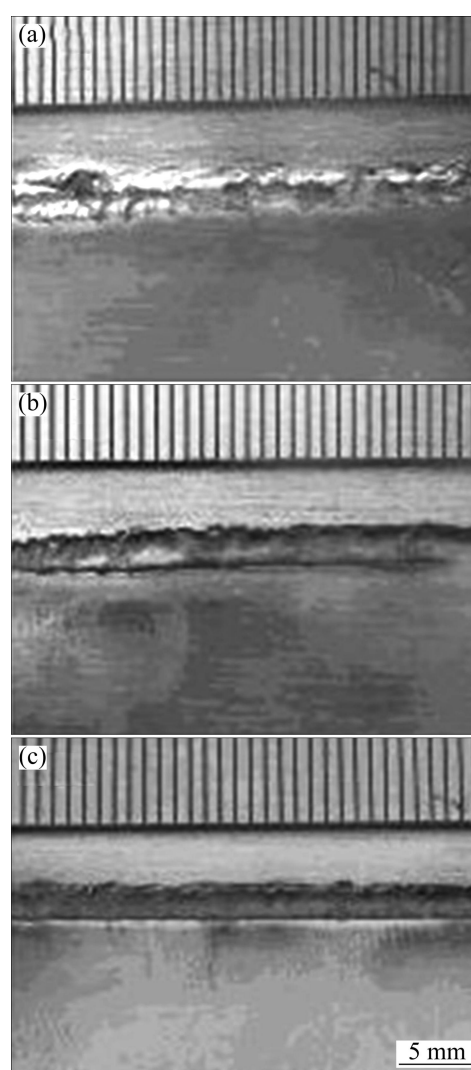


Fig. 1 SEM images showing morphology of seams under different beam offsets: (a) $d_s=0$; (b) $d_s=0.2$ mm; (c) $d_s=0.4$ mm

melted a lot. According to the binary phase diagram, Fe and Ag do not react with each other both at liquid and solid state, and the two liquid phases do not form symmetrical mixture, and the physical properties such as

fusion temperature and viscosity differ a lot from each other. So the morphology was not good.

With the movement of the beam spot to the silver side (Figs. 1(a) and (b)), the heat input of the steel side decreased rapidly as a result of the high energy density characteristic, and its fusion was reduced, and the melting pool became symmetrical in terms of both chemical composition and physical properties. So the morphology got much better.

3.2 Microstructure of seam under different beam offsets

Microstructures of the joints under different beam offsets are shown in Fig. 2. The dividing line between the steel and the correlative was quite obvious because of their exclusive characteristic from each other. The aluminum alloy was melted due to the heat conductivity of the Ag interlayer, and a transition layer was formed at the interface between them, and became thin and

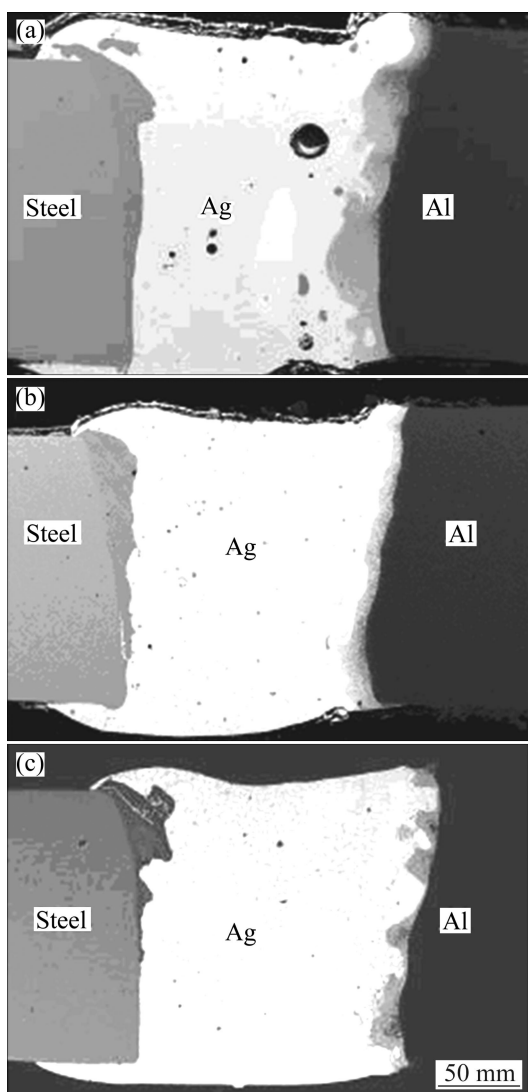


Fig. 2 SEM images showing microstructures of joints under different beam offsets: (a) $d_s=0$; (b) $d_s=0.2$ mm; (c) $d_s=0.4$ mm

spiccato with the increment of the beam offset. When the beam spot acted on the touching face of Ag interlayer and steel (Fig. 2(a)), a small part of the Ag interlayer distant from the beam spot did not melt. The joint froze fast as a result of the high heat conductivity of silver and aluminum, and porosity was formed because the metallic vapor did not have enough time to overflow. With the movement of the beam spot, the heat input at the Ag interlayer increased, which would help the vapor to overflow and thus eliminate the porosity. When d_s increased to 0.4 mm, the heat input on the steel side was so small that only the upper part melted a little, and more aluminum got melted and dissolved with the liquid silver.

3.3 Microstructure of seam under different beam offsets

The microstructure of the transition layer is shown in Fig. 3. According to the configuration of the layer and binary diagram of Ag and Al, we know that on the left side, there was mainly the eutectic composed of Ag_2Al IMC and Al, while on the right side, Al element took up a large ratio, and the microstructure was mainly Al, and some eutectic was also found on the crystal borders as a result of segregation. The microstructure compositions of the transition layer remained basically the same under different beam offsets. The microstructure of the interface between silver and steel under different beam offsets is shown in Fig. 4. The EDX results and probable phases are listed in Table 4.

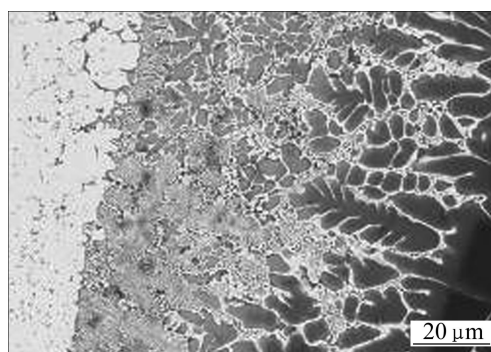


Fig. 3 SEM image showing microstructure of transition layer

When $d_s=0$ (Fig. 4(a)), only a little aluminum got melted, and the ratio of Al in the melting Fe was less than the solution limit, and unsaturated Fe was formed on the steel side of the interface. When $d_s=0.2$ mm (Fig. 4(b)), more aluminum got melted, the Fe–Al IMC layers were avoided to generate, and supersaturated Fe was formed. Those two factors will efficiently improve the joint strength. When $d_s=0.4$ mm (Fig. 4(c)), two IMC layers of FeAl and FeAl₃ respectively were formed on

the steel side, and some Fe–Al IMC particles appeared in the Ag interlayer.

3.4 Mechanical property of joints under different beam offsets

Figure 5 shows the tensile strength of the joints under different beam offsets. When $d_s=0.2$ mm, the maximum tensile strength of the joint was 193 MPa,

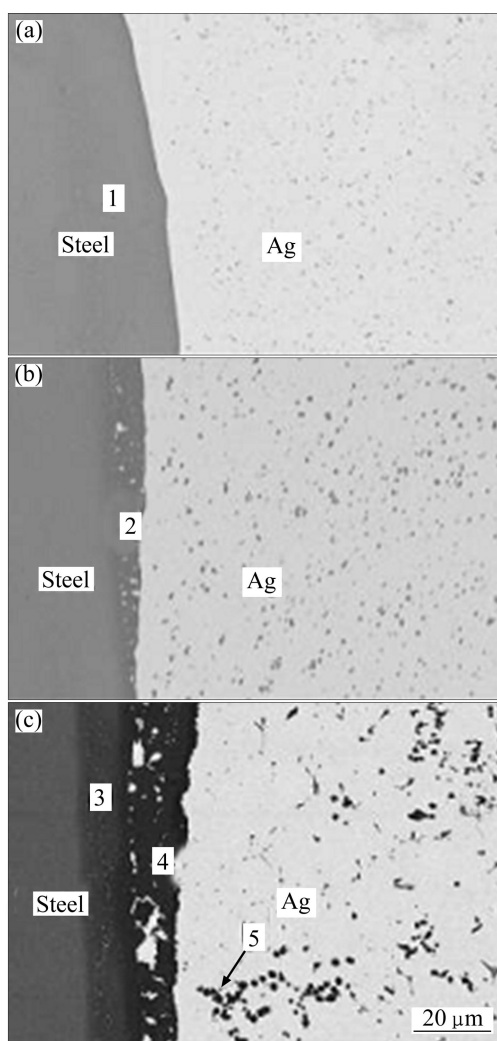


Fig. 4 SEM images showing microstructure of interface between silver and steel under different beam offsets: (a) $d_s=0$; (b) $d_s=0.2$ mm; (c) $d_s=0.4$ mm

Table 4 EDX results of points in Fig. 4 and probable phases

Point	x(Fe)/ %	x(Al)/ %	x(Ag)/ %	x(Cr)/ %	x(Ni)/ %	Probable phase
1	64.5	7.9	0.5	19.4	7.7	Non-saturated Fe
2	65.8	13.0	5.2	12.8	3.2	Over-saturated Fe
3	41.9	39.8	2.1	12.2	3.9	FeAl IMC
4	20.9	65.1	5.7	7.1	1.2	FeAl ₃ IMC
5	13.5	75.2	7.0	4.3	0	FeAl ₆ IMC

88.9% that of the aluminum alloy. When $d_s=0$, the seam morphology was bad, and porosity existed, so the strength was low relatively. When d_s was over 0.2 mm, Fe–Al IMC layers formed at the interface of steel/silver, resulting in the reduction of the strength. When $d_s=0.2$ mm, the heat input distribution was reasonable, the porosity was eliminated, and the Fe–Al IMC layers were not formed. So, the tensile strength of the joint was optimal.

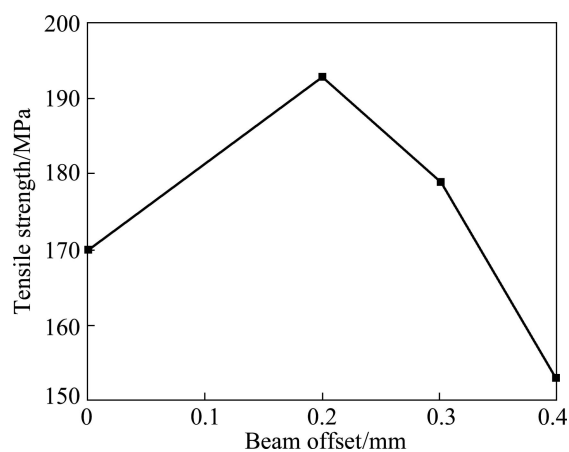


Fig. 5 Tensile strength of joints under different beam offsets

The morphology of the fracture of the optimal joint is shown in Fig. 6, and the EDX results and probable phases of the fracture are listed in Table 5. The fracture was divided into two parts with different characteristics: one was of cleavage-type fracture, and the EDX results indicated that it was supersaturated Fe zone; the other was of dimple-type fracture, and the EDX results indicated that it was supersaturated Ag zone. So, the fracture occurred at the interface between the steel and the Ag interlayer.

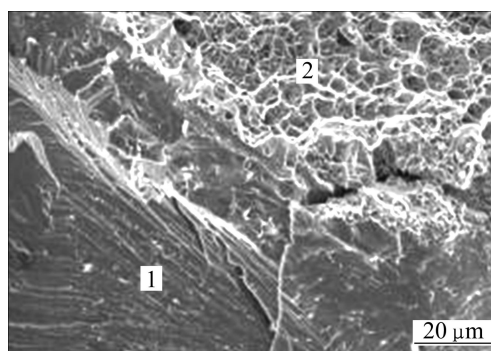


Fig. 6 SEM image showing morphology of fracture of optimal joint

Table 5 EDX results of points in Fig. 6 and probable phases of fracture

Point	x(Fe)/ %	x(Al)/ %	x(Ag)/ %	x(Cr)/ %	x(Ni)/ %	Probable phase
1	70.7	15.5	2.4	9.7	2.6	Supersaturated Fe
2	2.0	18.0	74.5	1.8	3.7	Supersaturated Ag

4 Conclusions

1) With the increment of the beam offset to the silver side from the touching face between Ag interlayer and steel, the seam morphology was improved, and the porosity in the Ag interlayer vanished.

2) A transition layer mainly composed of Ag_2Al and Al eutectic was formed at the interface between Ag interlayer and aluminum alloy, and became thin and spiccato as the beam offset increased. When the beam offset was too large, two IMC layers composed of FeAl and FeAl_3 respectively were formed at the interface between steel and Ag interlayer.

3) The optimal beam offset was 0.2 mm, and the maximum tensile strength of the joint was 193 MPa, 88.9% that of the aluminum alloy, and the fracture occurred on the interface between steel and Ag interlayer.

References

- [1] HARAGA K. Strength properties of aluminum/aluminum and aluminum/steel joints for light weighing of automotive body [J]. *Welding in the World*, 2000, 44(4): 23–27.
- [2] SCHUBERT E, KLASSEN M, ZERNER I, WALZ C, SEPOLD G. Light weight structures produced by laser beam joining for future applications in automobile and aerospace industry [J]. *Journal of Materials Processing Technology*, 2001, 115(1): 2–8.
- [3] LI H, HAN J T. Interlayer design and its effect on the liquid diffusion of steel-Al honeycomb sandwich panels [J]. *Journal of University of Science and Technology Beijing*, 2006, 28(2): 138–143.
- [4] GEIGER M, MICARI F, MERKLEIN M, FRATINI L, CONTORNO D, GIERA A, STAUD D. Friction stir knead welding of steel aluminum butt joints [J]. *International Journal of Machine Tools and Manufacture*, 2008, 48(5): 515–521.
- [5] WATANABE T, TAKAYAMA H, YANAGISAWA A. Joining of aluminum alloy to steel by friction stir welding [J]. *Journal of Materials Processing Technology*, 2006, 178: 342–349.
- [6] UZUN H, DONNE C D, ARGAGNOTTO A, GHIDINI T, GAMBARO C. Friction stir welding of dissimilar Al 6013-T4 to X5CrNi18-10 stainless steel [J]. *Materials and Design*, 2005, 26(1): 41–46.
- [7] YOKOYAMA T. Impact tensile properties of 6061 aluminum alloy to SUS 304 stainless steel friction-welded butt joints [J]. *Welding International*, 2003, 17(7): 514–523.
- [8] LIU P, LI Y J, WANG J, GUO J S. Vacuum brazing technology and microstructure near the interface of Al/18-8 stainless steel [J]. *Materials Research Bulletin*, 2003, 38(9–10): 1493–1499.
- [9] MATHIEU A, PONTEVICCI S, VIALA J, CICALA E, MATTEI S, GREVEY D. Laser brazing of a steel/aluminum assembly with hot filler wire (88% Al, 12% Si) [J]. *Materials Science and Engineering A*, 2006, 435–436: 19–28.
- [10] HE P, FENG J C, QIAN Y Y, HUANG Z F, MAI H H. Resolve of fragile and reaction defect problem for a new contact reaction brazing aluminum to stainless steel [J]. *Materials Science & Technology*, 2005, 13(1): 82–85.
- [11] LÜ X Q, SHI Z X, YANG S L, WU Y X. The process and principle analysis of Ni/Cu transitional layer brazing of Al (Al alloys) and stainless steel [J]. *Materials for Mechanical Engineering*, 2004, 28(1): 23–25.
- [12] ZHANG H T, FENG J C, HE P, HACKL H. Interfacial microstructure and mechanical properties of aluminum-zinc-coated steel joints made by a modified metal inert gas welding-brazing process [J]. *Materials Characterization*, 2007, 58(7): 588–592.
- [13] SONG J L, LIN S B, YANG C L, MA G C, LIU H. Spreading behavior and microstructure characteristics of dissimilar metals TIG welding-brazing of aluminum alloy to stainless steel [J]. *Materials Science and Engineering A*, 2009, 509(1–2): 31–40.
- [14] LEI Z, QIN G L, LIN S Y, WANG X Y, WANG W. Fusion-brazing welding for dissimilar metals between aluminum and steel by Nd:YAG laser-MIG hybrid welding [J]. *Welding*, 2006, 6: 36–37.
- [15] LEI Z, QIN G L, LIN S Y, WANG X Y. Fusion-brazing joining for dissimilar metals between 5A02 aluminum alloy and zinc-coated steel based on laser-MIG hybrid welding [J]. *Journal of Mechanical Engineering*, 2009, 45(3): 94–98.

铝合金/Ag 中间层/钢的电子束偏束焊接头组织与性能

张秉刚¹, 陈国庆¹, 张春光¹, 倪家强²

1. 哈尔滨工业大学 先进焊接与连接国家重点实验室, 哈尔滨 150001;

2. 中航工业沈阳飞机工业(集团)有限公司, 沈阳 110034

摘要: 在铝合金与钢之间添加 Ag 中间层后进行电子束焊接实验。其他参数固定的情况下, 对电子束作用位置不同时的焊缝成形、接头组织和力学性能进行分析。结果表明: 随着电子束斑点从银-钢对接面向银侧偏移距离的增大, 焊缝成形明显得到改善, 接头中的气孔缺陷消失。在银-铝对接面形成由 Ag_2Al 和 Al 共晶组成的过渡层, 过渡层随着偏束距离的增大而变窄且不连续。当偏束距离过大时, 在银-钢界面上形成 FeAl 和 FeAl_3 两种化合物层。当电子束最佳偏束距离为 0.2 mm 时, 接头强度最高达 193 MPa, 为铝母材的 88.9%, 此时断裂发生在银-钢界面上。

关键词: 铝合金; 钢; Ag 中间层; 电子束偏束焊; 接头

(Edited by YANG Hua)